

# Dust release from surfaces exposed to plasma

T. M. Flanagan<sup>a)</sup> and J. Goree

*Department of Physics and Astronomy, The University of Iowa, Iowa City, Iowa 52242*

(Received 24 August 2006; accepted 30 October 2006; published online 14 December 2006)

Micrometer-sized particles adhered to a surface can be released when exposed to plasma. In an experiment with a glass surface coated with lunar-simulant dust, it was found that particle release requires exposure to both plasma and an electron beam. The dust release rate diminishes almost exponentially in time, which is consistent with a random process. As proposed here, charges of particles adhered to the surface fluctuate. These charges experience a fluctuating electric force that occasionally overcomes the adhesive van der Waals force, causing particle release. The release rate increases with plasma density, so that plasma cleaning is feasible at high plasma densities. Applications of this cleaning include controlling particulate contamination in semiconductor manufacturing, dust mitigation in the exploration of the moon and Mars, and dusty plasmas.

© 2006 American Institute of Physics. [DOI: [10.1063/1.2401155](https://doi.org/10.1063/1.2401155)]

## I. INTRODUCTION

Small particles of solid matter, or dust, that are adhered to a surface can be released from the surface when exposed to a plasma. The release process, which has also been called plasma cleaning or shedding, is of interest in several fields including particulate contamination in semiconductor manufacturing,<sup>1,2</sup> tritium retention by dust in fusion devices, dust mitigation for lunar exploration, and the natural phenomenon of moon dust levitation in geophysics.<sup>3</sup>

Dust release from a surface occurs because, when exposed to a plasma, dust particles become charged. These charged particles are exposed to the plasma's sheath electric field, resulting in an electric force. This was demonstrated experimentally by Sheridan *et al.*<sup>4</sup> A sample was coated with alumina dust and placed in a vacuum chamber where it was exposed to a discharge plasma. The results reported suggested that dust is released from the surface at a rate that varies in time as an inverse exponential. However, the data did not allow drawing a firm conclusion for the time dependence because plasma conditions were purposely altered during the course of the experiment.

In this paper, we report results of dust-release tests where a glass surface is coated with dust particles and exposed to a discharge plasma. We seek to identify conditions that are necessary for dust release, to verify that the rate of release varies with time as an inverse exponential, and to determine how the time constant for this exponential variation depends on plasma parameters, in particular the plasma density.

Our experimental method is modeled after that of Sheridan *et al.*,<sup>4</sup> using the same method of sample preparation and the same time-resolved measurement of the dust release rate. The main difference is that here we hold plasma conditions constant through the duration of tests to better observe the time dependence. In addition, we use video imaging of the dust release as an extra diagnostic. Further, we use a different dielectric dust, lunar simulant JSC-1, to coat the sample's

surface. The reasoning is that our results could be useful for designing dust mitigation schemes in future missions to the moon, for example. This simulant, described later in this paper, was manufactured in the 1990s by researchers working with NASA's Johnson Space Center (JSC), to mimic moon dust.

One of the most important factors in dust release is certainly the charge on dust particles adhered to a surface that is exposed to a plasma. Previous studies have been done on the charging of isolated dielectric dust grains,<sup>5,6</sup> including JSC-1 simulant,<sup>7,8</sup> in a discharge plasma under high vacuum and at gas pressures near 1 mTorr. In these experiments, charging of dust particles for different particle sizes were studied, and results showed that for an isolated dust particle falling through a plasma, a capacitive charging model could be applied. Other experiments investigated the charging of JSC-1 dust particles while they were attached to metal surfaces<sup>9,10</sup> and the results, on average, showed that the charge on dust particles could be predicted by treating the dust as isolated spherical capacitors. In these tests, the distance separating dust particles on the surface was much larger than the size of the dust particles, so that pair interactions between dust particles were not important.

Here, we report experiments in which the particles' charge cannot be accurately modeled merely by assuming that the particle is an isolated sphere immersed in a plasma. We prepared a sample with particles attached to a surface. Moreover, we applied a thicker coating of dust to our surface so that not only were particles adhered to the solid surface, but some were adhered instead to other particles on the surface. In Sec. II we will discuss how these conditions complicate estimating the charge on a particle.

Our main results are measurements of the dust release rate, which suggest there is a fluctuating mechanism that may play a role in dust release. We verified that the release rate diminishes exponentially with time as dust is depleted from the surface, and we find that the exponential time constant varies with the plasma density accurately to a power law, as presented in Sec. V. The exponential time dependence

<sup>a)</sup>Electronic mail: timothy-flanagan@uiowa.edu

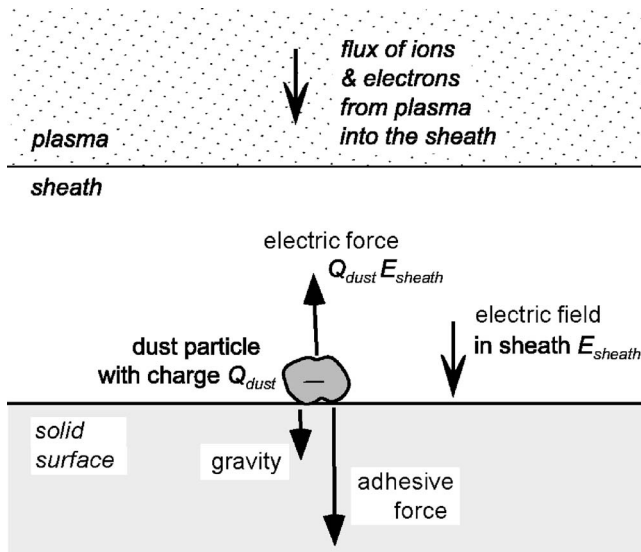


FIG. 1. (Color online) Sketch of the three forces acting on a dust particle attached to a surface immersed in a plasma. The adhesive force is a van der Waals force  $F_{\text{VDW}}$ , which is opposed by the electric force  $Q_{\text{dust}}E_{\text{sheath}}$ . This drawing is not to scale. In our experiment, the dust particle size is less than 20  $\mu\text{m}$ , and the sheath thickness is greater than 5 mm.

suggests that some random fluctuation plays a role in dust release, as we discuss in Sec. VI. These results will be useful in planning the conditions required to use plasma cleaning in semiconductor manufacturing and in exploration of the moon and Mars.

## II. FORCES ACTING ON A DUST PARTICLE

In this section, we review the forces acting on a particle adhered to a surface while immersed in a plasma, illustrated in Fig. 1. These include the adhesive van der Waals force, the repulsive electric force, and less importantly gravity. We describe the forces conceptually, present models for estimating them, and identify the validity or limitations of these models. The electric force  $Q_{\text{dust}}E_{\text{sheath}}$  depends on the particle charge  $Q_{\text{dust}}$ , which is complicated to model, as well as the sheath electric field at the surface  $E_{\text{sheath}}$ , which can be modeled more easily. The van der Waals force depends sensitively on a parameter that is either difficult or impractical to measure.

### A. Adhesive van der Waals force

First, we discuss the adhesive van der Waals force, which is the force that must be overcome to release particles from a surface. This force arises from incoherent, randomly fluctuating dipoles between molecules or atoms.<sup>11</sup> These dipole fluctuations at the molecular level result in an interaction between two or more macroscopic objects, which here are dust particles or the surface. Random directions in polarization cause cancellation; therefore, the van der Waals force scales linearly with the size of the dust particle instead of scaling as the particle's surface area, which might be more intuitive. The dipole fluctuations are usually dominated by frequencies in the ultraviolet range or higher,<sup>12</sup> so they can occur on time scales of  $\sim 10^{-16}$  s or faster.

A commonly used model for estimating the van der Waals force  $F_{\text{VDW}}$  is the Hamaker model. In addition to the size of the dust particles,  $F_{\text{VDW}}$  also depends on the distance between the two interacting objects, referred to as the contact distance  $D$ . A third parameter called the Hamaker constant  $A$  is a material property of the two interacting objects that has units of energy. The specific form of  $F_{\text{VDW}}$  in the Hamaker model depends on the geometry of the interacting objects. For the simple case of the interaction between two spheres of radius  $R_1$  and  $R_2$ , the result<sup>11</sup> is

$$F_{\text{VDW}} = \frac{A}{6D^2} \frac{R_1 R_2}{R_1 + R_2}. \quad (1)$$

The Hamaker constant  $A$  does not depend on particle morphology, nor does it vary greatly among different materials; it is usually in the range of  $(0.4\text{--}4) \times 10^{-19}$  J. The contact distance  $D$ , however, is generally known with much less precision. For smooth particles, the contact distance is typically about 0.3 nm.<sup>11</sup> Using this contact distance with a typical particle radius of 1  $\mu\text{m}$  gives  $F_{\text{VDW}} \approx 10^{-7}$  N. However, JSC-1 particles are not smooth and using a contact distance this small would overestimate the van der Waals force. To model rough particles, we will follow the practice of using a larger value of  $D$  that corresponds to a typical asperity size on the particle that is due to roughness.<sup>13</sup> As an example, if we use an asperity size that is 10% of the 1  $\mu\text{m}$  particle radius, then the adhesive force is roughly  $F_{\text{VDW}} \approx 10^{-12}$  N. An alternative method of modeling rough particles,<sup>14</sup> not used here, is to calculate a range of values for the van der Waals force by modeling the input parameters  $A$ ,  $R_1$ ,  $R_2$ , and  $D$  as a distribution rather than single values.

We did not attempt a direct measurement of  $F_{\text{VDW}}$  for JSC-1 grains, and therefore our estimates of the van der Waals force have significant uncertainty. Other experimenters have developed techniques for measuring the van der Waals force, including using a centrifuge or an atomic force microscope.<sup>15</sup> These techniques require specialized equipment that were not available for this experiment.

### B. Electric force

Next, we review the electric force that acts on a particle adhered to a surface immersed in a plasma. This force can overcome adhesion and thereby cause a release of dust from the surface. In fact, this is the only force that can account for dust release in the experiment that we will describe. If the dust charge is negative and the electric field points toward the surface, then the electric force will be directed away from the surface. Thus, it acts opposite to the adhesive van der Waals force. We will first discuss models of the dust charge and then the electric field.

#### 1. Charge

The charge  $Q_{\text{dust}}$  of a small dust particle must be considered along with the charge of the larger surface that it is adhered to. Because of this complication, there is no single obvious model for calculating the charge on a dust particle.

Regardless of the model, we can describe a dust particle's charge as the sum of a time-averaged value  $\overline{Q}_{\text{dust}}$  and a fluctuating value  $\delta Q_{\text{dust}}$  so that

$$\overline{Q}_{\text{dust}}(t) = \overline{Q}_{\text{dust}} + \delta Q_{\text{dust}}(t). \quad (2)$$

For the time-averaged charge  $\overline{Q}_{\text{dust}}$ , we will describe two extreme cases that we term the "isolated capacitors" model and the "shared charge" model. These extreme models are useful because they can provide limiting values for the charge on a dust particle, where the actual charge is between them. Both of these models are static, neglecting any temporal fluctuations of the charge, as we will discuss later.

The isolated capacitors model, which yields a much larger estimate of the time-averaged dust charge, assumes that each dust particle is charged as if it were an isolated sphere immersed in a plasma, neglecting the effects of the nearby surface. The dielectric particle is treated as a capacitor even though the concept of capacitance applies only to conductors. Electrons and ions deposit their charge at their point of impact with the dielectric surface. For a dielectric, these charges are unable to rearrange themselves afterward to form an equipotential, as they would do on the surface of a conductor. However, if the dielectric particle has spherical symmetry, the random impacts of electrons and ions on the surface of the particle will be distributed uniformly, so that an isolated dielectric sphere can be modeled as if it were a spherical capacitor. The charge on the spherical dust particle is then given by

$$\overline{Q}_{\text{dust}} = C_{\text{dust}} \overline{V}_{\text{float}} = 4\pi\epsilon_0 a_{\text{dust}} \overline{V}_{\text{float}}, \quad (3)$$

where  $C_{\text{dust}}$  is the usual capacitance of a sphere,  $a_{\text{dust}}$  is the radius of the spherical particle, and  $\overline{V}_{\text{float}}$  is the time-averaged floating potential of the dust particle referenced to the plasma potential. The floating potential is the potential at which the total current to a surface, from collection of electrons and ions, is zero. This model is very commonly used to estimate the charge of isolated dust particles immersed in a plasma (not in contact with a surface), for example in experimental studies on dust grain charging<sup>16,17</sup> and sheath modification due to dust.<sup>18</sup>

Our shared charge model, which yields a much lower estimate of the dust charge, treats the dusty surface, which we will refer to as the sample, as a single spherical capacitor of charge  $Q_{\text{sample}}$ , so that an individual dust particle merely shares the total charge  $Q_{\text{sample}}$  according to its share of the sample's total surface area. A larger dust particle will have a larger charge according to the square of its radius

$$\overline{Q}_{\text{dust}} = Q_{\text{sample}} \frac{a_{\text{dust}}^2}{a_{\text{sample}}^2}, \quad (4)$$

where  $a_{\text{sample}}$  is the radius of the dusty sample. The charge  $Q_{\text{sample}}$  of the entire dusty surface is

$$Q_{\text{sample}} = 4\pi\epsilon_0 a_{\text{sample}} V_{\text{float}}. \quad (5)$$

Samples are often so large, as in our experiments, that the percentage temporal fluctuations are negligible compared to the time-averaged charge,<sup>19</sup> unlike the situation for the small dust particle, which can have much larger percentage fluc-

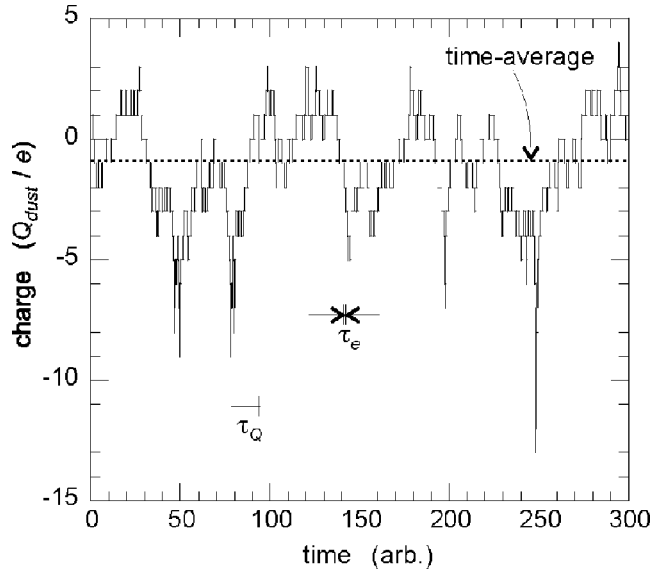


FIG. 2. Conceptual illustration of charge fluctuations for a dust particle attached to a surface. The dust charge  $Q_{\text{dust}}$  changes by either  $+e$  or  $-e$  whenever an ion or electron is collected at random time intervals, with a typical time scale  $\tau_e$ . We propose that dust release from the surface occurs only when the charge fluctuates to a large value, which would occur infrequently with a long time scale  $\tau_Q$ . The time series shown here was prepared for an arbitrarily chosen stochastic process that does not quantitatively model the actual charging process in the experiment, and is intended only to illustrate the concepts.

tuations. At any time, the total charge on the system of the glass surface coated with dust is

$$Q_{\text{total}} = Q_{\text{glass}} + \sum_i Q_{\text{dust}_i} = Q_{\text{sample}}, \quad (6)$$

where  $Q_{\text{glass}}$  is the charge on the glass surface and  $Q_{\text{dust}_i}$  is the charge on the  $i$ th dust particle that is adhered to the glass surface or other dust particles.

In this shared charge model, Eq. (6) is very reliable, but Eq. (4) has the significant limitation that it predicts only a time-average value, and ignores the temporal fluctuations. Individual electrons and ions will be collected by dust particles at random time intervals so that the actual charge of a dust particle will fluctuate around a time-averaged value, as sketched qualitatively in Fig. 2. Modeling the fluctuating part  $\delta Q_{\text{dust}}$  would require a theory for the currents collected by a particle on the surface, which is likely to depend on the potential of the particle and the potentials of nearby particles and surfaces. We have no such theory, although we note that it is likely to be a stochastic fluctuation about a mean value. We propose that the instantaneous charge of a dust particle can be significantly larger than the time-averaged value, which will usually be less than the charge of one electron.

In considering these two models for estimating  $Q_{\text{dust}}$ , each has its own flaws. The isolated capacitors model overestimates the charge on a dust particle because the total charge on the system of the dusty sample  $Q_{\text{total}}$  is limited roughly by the charge on the sample  $Q_{\text{sample}}$ . If the sample were to charge to a potential that was much less than  $V_{\text{float}}$ , then ions would be attracted to the surface, electrons would be repelled, and thus the surface potential of the sample

would be restored back toward  $\bar{V}_{\text{float}}$ . A similar argument applies if the sample were to charge to a potential that was much greater than  $\bar{V}_{\text{float}}$ . Thus, if each dust particle simultaneously charged according to the isolated capacitors model, the total charge on the sample would be too great and would not satisfy Eq. (6). On the other hand, the shared charge model does satisfy Eq. (6), but still it only yields a prediction of the time-averaged charge.

## 2. Electric field

The electric field experienced by a particle while adhered to the surface has two contributions, one at a microscopic scale arising from pair interactions between individual dust particles, and the other from the macroscopic sheath that forms naturally between the sample's surface and the plasma. The microscopic electric field might play an important role, especially because it can fluctuate as we discuss later, but we have no quantitative model to predict this microscopic electric field. However, the macroscopic electric field due to the plasma's sheath can be modeled more reliably.

The sheath electric field is modeled by assuming a time-independent, collisionless, and planar sheath as in Sheridan and Goree,<sup>20</sup> with a slight modification. These assumptions are appropriate for the experiment described in the following sections, and we therefore believe that the electric field predicted using this model is sufficiently accurate. The electrons are modeled as having two thermal components of lower and higher energy, which are referred to as *cold* and *hot*, respectively, in order to better model our experiment. Langmuir probe data are used to determine  $V_{\text{float}}$  and the plasma parameters  $n_{\text{cold}}$ ,  $n_{\text{hot}}$ ,  $T_{\text{cold}}$ , and  $T_{\text{hot}}$ , where each refers to the plasma number density and temperature of their respective electron component, which will be discussed further in Sec. IV. By following the same treatment as Sheridan and Goree,<sup>20</sup> with the exception of an extra term in the electron density, an equation is easily derived for the sheath electric field evaluated at the surface

$$E_{\text{sheath}} = -\sqrt{2} \frac{T_{\text{cold}}}{e\lambda_{\text{cold}}} \left\{ \left( 1 + \frac{n_{\text{hot}}}{n_{\text{cold}}} \right) \times M^2 \left( \sqrt{1 - \frac{2}{M^2} \frac{eV_{\text{float}}}{T_{\text{cold}}}} - 1 \right) + \exp\left(\frac{eV_{\text{float}}}{T_{\text{cold}}}\right) - 1 + \frac{n_{\text{hot}}T_{\text{hot}}}{n_{\text{cold}}T_{\text{cold}}} \left[ \exp\left(\frac{eV_{\text{float}}}{T_{\text{hot}}}\right) - 1 \right] \right\}^{1/2}, \quad (7)$$

where,  $\lambda_{\text{cold}}$  is the Debye length of the cold electron component,  $e$  is the electron charge, and  $M$  is the Mach number, which is typically unity or slightly larger. The leading minus sign indicates that the sheath electric field is directed toward the sample. In calculating the electric field using a sheath model, we neglect the small correction for the nonplanarity of the sheath around the spherical sample because there are more significant uncertainties in computing the van der Waals forces, which competes with the electric force due to this electric field.

## 3. Gravity

Gravity is also a force that acts on a dust particle, but it is easy to understand that it is insignificant because particles adhered to a surface generally do not fall off when the surface is inverted. However, calculating the force of gravity is helpful because it provides a reliable lower limit on the van der Waals force. For a spherical dust particle of radius 1  $\mu\text{m}$ , the force of gravity would be about  $10^{-13}$  N.

## 4. Fluctuations and release

An important issue regarding all the forces acting on a dust particle is that only the electric force fluctuates. If all forces are steady, then particles should be released from the surface all at once when first exposed to a plasma, or not at all. However, if one of the forces fluctuates, then dust particles could be released gradually according to Poisson statistics. We certainly know that the force of gravity on a particular dust grain is not fluctuating. The magnitude of the adhesive force on a particular dust grain may fluctuate, but we know that this cannot by itself cause dust release because we do not see dust release without the presence of a plasma. On the other hand, the electric force can fluctuate, due to either a fluctuation in  $Q_{\text{dust}}$  or the electric field at the surface. It is well known that the dust charge  $Q_{\text{dust}}$ , and thus the electric force, fluctuates due to collecting discrete electrons and ions at random intervals, as explained above. The electric field at the surface consists partly of the sheath field  $E_{\text{sheath}}$  that does not fluctuate due to the large size of the sample. In principle, microscopic electric fields associated with dust-dust interactions on the surface could fluctuate, but we have no way to model this, or determine whether it could be significant.

We propose that a stochastically fluctuating charge  $Q_{\text{dust}}$  accounts for the dust release. Our argument supporting this proposed mechanism is provided in Sec. VI.

Once a negatively charged dust particle has been released from the surface, it will not return to the surface, because the sheath electric field will continue to accelerate the particle away from the sample's surface. This is due to the different dependence of the van der Waals force and the electric force on the particle's separation from the sample's surface. The van der Waals force decreases rapidly, i.e.,  $\propto D^{-2}$ , while the electric force decreases much more slowly with distance; it diminishes with a scale length  $\lambda_D$  which is about three orders of magnitude larger than a typical contact distance  $D$ . For example, for a 1  $\mu\text{m}$  radius dust particle, we calculate that  $F_{\text{VDW}}$  is reduced by a factor of 10 by increasing  $D$  from 0.1 to 0.3  $\mu\text{m}$ , while a similar tenfold reduction of the electric force occurs only after a much larger 5 mm separation from the surface.

## III. EXPERIMENTAL CONCEPT

Here we describe the requirements for an experiment intended to identify the conditions required for dust particle release and to measure the rate of release. As we will show later, measuring the time series for dust release and how the release rate varies with plasma density is useful for revealing the cause of dust release. Recording this time series requires

an *in situ* measurement, which can be accomplished using laser-light scattering (LLS). To identify the conditions required for dust release, we will report our measurements for three conditions:

- (1) an electron beam with no plasma,
- (2) a plasma with no electron beam,
- (3) a plasma with an electron beam.

We chose to operate at a low gas pressure so that we can use the simple collisionless sheath model to compute the macroscopic sheath electric field  $E_{\text{sheath}}$ . This requires operating at sufficiently low gas pressure so that the mean free paths for electron-impact ionization and ion-neutral collisions are both much larger than the sheath thickness. At a pressure of 1 mTorr, the mean free path for electron-impact ionization is about 1400 cm and the mean free path for symmetrical charge-transfer between Ne and  $\text{Ne}^+$  is about 14 cm. These values are significantly larger than the sheath thickness. The sheath thickness is characterized by the Debye length, which is  $<10$  mm for almost all types of laboratory plasmas.

We chose materials and methods relevant to the application of cleaning space suits and other dusty surfaces in future lunar habitats. To mimic moon dust, we used JSC-1 lunar simulant, and we used a glass surface to model dielectric surfaces on space suits and habitats. To test a cleaning method that could be used on the moon, we operate with plasma conditions that could be achieved with a variety of different plasma sources, and in vacuum conditions that could be achieved, for example, in an airlock.

#### IV. APPARATUS

To study dust release, we used a sample consisting of a glass sphere coated with dust. The hollow glass sphere is 4.5 cm in diameter and is uniformly coated with dust for each test. During each test, this sample rotates on a horizontal axis with a period of about 4.7 s so that most of the sample's surface area is exposed to the electron beam. Further, the sample is electrically floating, just as most objects would be in a lunar or Martian habitat.

The dust used to coat the sample is JSC-1 lunar simulant, which mimics lunar samples returned by Apollo missions. JSC-1 is a mineral powder that was mined from volcanic ash. It is quite similar to lunar soil samples in density, chemical composition, mineralogy, size distribution,<sup>21,22</sup> and elasticity.<sup>23</sup> The mass density of JSC-1 is typically  $2.9 \text{ g/cm}^3$ ,<sup>21</sup> which is useful for estimating the force of gravity and the number of dust particles on the surface. Willman *et al.*<sup>22</sup> reported that JSC-1 has a polydisperse size distribution including particles smaller than  $1 \mu\text{m}$ . We modify the simulant in two ways to make it more suitable for this experiment. First, we use a permanent magnet to remove most of the ferromagnetic particles to avoid harming our equipment. Second, we sieve the powder to eliminate particles larger than  $20 \mu\text{m}$ . Limiting the particle size is desirable because small particles are generally thought to pose the greatest challenge in cleaning surfaces, such as woven space

suits or semiconductor manufacturing materials with submicrometer features.

An electrostatic method is used to coat the glass sphere with dust in a reproducible manner, using the same method as Sheridan *et al.*<sup>4</sup> A low-power Van de Graaff generator is used to bias the sphere to a high potential. The sphere is then held over a petri dish containing JSC-1. Electrostatic attraction picks up dust, which remains attached by adhesion. This method allows us to consistently prepare samples with 60–80 mg of JSC-1 dust. The electrostatic method provides a more uniform and repeatable coating than simpler methods such as placing the sample into a plastic bag filled with dust and shaking it. After coating the surface, we expose the sample to air overnight so that atmospheric water vapor neutralizes the residual charge. We did not determine whether water vapor during atmospheric exposure affects adhesion. At this point the sample is no longer charged, and we introduce it into a vacuum chamber, where it is mounted on a motorized rotating shaft.

The coating of dust is thin, with a few layers of dust particles on the surface. As an estimate of the interparticle spacing on a sample, we assume that all dust particles are  $1 \mu\text{m}$  diameter spheres. For a sample with 70 mg of dust, we calculate that there would be about  $10^9$  dust particles distributed over the sample's surface area of  $6.4 \times 10^9 \mu\text{m}^2$ . Comparing these two values, we estimate that the sample is coated with a few layers of dust and that a dust particle is either adhered to the glass, or to another dust particle.

The vacuum chamber is divided into two sections, as shown in Fig. 3, with a smaller source chamber and a larger test chamber where the sample is mounted. The test chamber, which has inner dimensions of 32.4 cm diameter and 31.6 cm height, is black-anodized to reduce unwanted light scattering. The vacuum chamber base pressure is typically  $2 \times 10^{-6}$  Torr using a turbomolecular pump.

As a first step for plasma operation, gas is admitted to a desired pressure. We note that this step is similar to partially venting an airlock. Thus, our vacuum chamber can be considered as a proxy for an airlock for the purpose of simulating plasma cleaning methods for use on the moon or Mars. We chose to use neon gas because it has no spectral lines near the wavelengths we used for LLS.

The plasma source generates both a low-temperature plasma and an electron beam. The plasma is sustained by electron-impact ionization using primary electrons emitted in the source chamber. Tungsten filaments in the source chamber are heated with a power supply so that they are emissive. The plasma is turned on at the desired time by suddenly applying a dc bias to the filaments of  $-70$  V with respect to the grounded walls of both sections of the vacuum chamber. The electrons emitted from the filaments are the primary electron beam. In addition to the electrons in the primary electron beam (hereafter referred to as the electron beam), there are also thermal electrons and ions produced when gas is introduced and partially ionized by electron impact.

To adjust the plasma density  $n$  in the test chamber over a wide range we used two means: one fine and one coarse. By varying the heating current to the tungsten filaments, we vary the electron emission, providing a fine adjustment of the

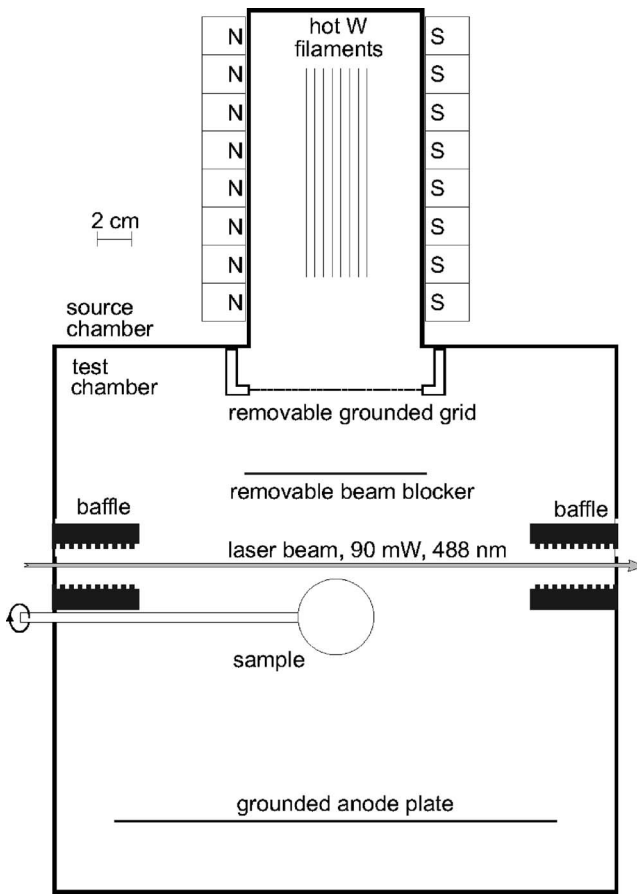


FIG. 3. Scale drawing of the experimental apparatus, shown from the side. A plasma is created by electron-impact ionization of neon gas. In the source chamber, primary (beam) electrons are emitted from heated tungsten filaments that are biased negatively to  $-70$  eV. The upper hemisphere of the sample faces the electron beam, which can be blocked when desired by a removable metal plate (beam blocker). The sample rotates with a  $4.7$  s period to avoid exposing only one portion of the sample to the electron beam. Dust release from the sample is detected by laser-light scattering of a laser beam located just above the sample's surface.

plasma density. Additionally, we either insert or remove a grounded wire-mesh grid between the source chamber and the main chamber, as shown in Fig. 3. When inserted, the grid reduces the plasma density in the main chamber by more than an order of magnitude. Using these two adjustments, we vary the plasma density  $n$  by more than two orders of magnitude, up to  $2.5 \times 10^8 \text{ cm}^{-3}$ .

Plasma density and temperature were measured using a Langmuir probe. All of the measurements reported here were made in the absence of dust, but otherwise with the same operating conditions. It is possible that when dust is released into the plasma, the electron density will be depleted to levels below those reported here.<sup>24</sup> The Langmuir probe has a planar tantalum tip of diameter  $11.07$  mm and a thickness of  $0.23$  mm. As in Sheridan *et al.*,<sup>4</sup> we make Langmuir probe measurements without the sample installed.

All the measurements for a plasma with an electron beam reveal that instead of having a single temperature, the thermal electrons in the test chamber can be characterized as having two Maxwellian components with temperatures  $T_{\text{hot}}$  and  $T_{\text{cold}}$ . Thus, the two-temperature sheath model described

above in Sec. II B 2 will be suitable for this application. With the grid in place,  $T_{\text{cold}}$  ranged from  $0.3$  to  $0.5$  eV, and  $T_{\text{hot}}$  ranged from  $3$  to  $4$  eV. With the grid removed,  $T_{\text{cold}}$  ranged from  $3$  to  $4$  eV, and  $T_{\text{hot}}$  ranged from  $12$  to  $16$  eV. The density of the primary electron beam could not be estimated with the Langmuir probe under conditions with a plasma.

Langmuir-probe measurements for a plasma without an electron beam indicated generally the same values for  $n$ ,  $T_{\text{cold}}$ , and  $T_{\text{hot}}$  as for a plasma with an electron beam. The electron beam is responsible for sustaining ionization throughout most of the vacuum chamber, but it is obstructed by a beam blocker (see Fig. 3) so that it does not impinge on the sample or, for this measurement, the Langmuir probe.

For the conditions with an electron beam only, the Langmuir probe charges to a floating potential that is about the same as the  $70$  eV electron beam, indicating that the sample with its dust coating would similarly charge to that potential. There is no significant plasma sheath surrounding the sample for the exceedingly low plasma density at these conditions.

Because the plasma density  $n$  is the main plasma parameter that was varied, we verified our Langmuir-probe measurements of  $n$  using two methods of calculating the plasma density for the same  $I$ - $V$  curve. As the first method,  $T_{\text{hot}}$ ,  $T_{\text{cold}}$ , and the number density of thermal electrons,  $n_{\text{hot}}$  and  $n_{\text{cold}}$ , were determined by fitting the electron current to the sum of currents from the hot and cold electron distribution functions, in the region of the  $I$ - $V$  curve where electrons are repelled.<sup>25</sup> The plasma density for this method is  $n_{\text{hot}} + n_{\text{cold}}$ . As the second method, the electron energy distribution function was used. This method assumes no specific form for the electron distribution function, but only that it is isotropic, and involves computing a moment of the second derivative of the  $I$ - $V$  curve.<sup>26</sup> The two methods agreed reasonably well and the plasma density was calculated as the average of their results.

Since charging of the sample is thought to be an essential requirement for particle release, we observed, as a proxy for the sample, the charging of a floating Langmuir probe. For conditions with both a plasma and an electron beam, we observed a floating potential  $V_{\text{float}}$  of typically  $-4$  to  $-10$  V with the grid in place, and  $-14$  to  $-35$  V without the grid. For conditions with a plasma only, the floating potential of the Langmuir probe was about the same as for a plasma with an electron beam. As discussed in Sec. II, the charge  $Q_{\text{sample}}$  on the dust sample as a whole can be calculated as  $4\pi\epsilon_0 a_{\text{sample}} V_{\text{float}}$ .

There is a flux of thermal electrons and ions to the sample's surface when it is exposed to a plasma, and the flux of course increases with plasma density  $n$ . This is significant, among other reasons, because the time scale for the charge of individual dust particles to vary stochastically will be inversely proportional to the flux. For our experiment, the number flux of electrons ranged from  $3.4 \times 10^{11} \text{ cm}^{-2} \text{ s}^{-1}$  at our lowest plasma density of  $n = 2.4 \times 10^6 \text{ cm}^{-3}$ , to  $1.1 \times 10^{14} \text{ cm}^{-2} \text{ s}^{-1}$  at our highest plasma density of  $n = 2.5 \times 10^8 \text{ cm}^{-3}$ .

Our laser-light scattering setup, shown in Fig. 4, provides time-resolved measurements of the dust release rate as well as video images of the release as it occurs. A  $90$  mW

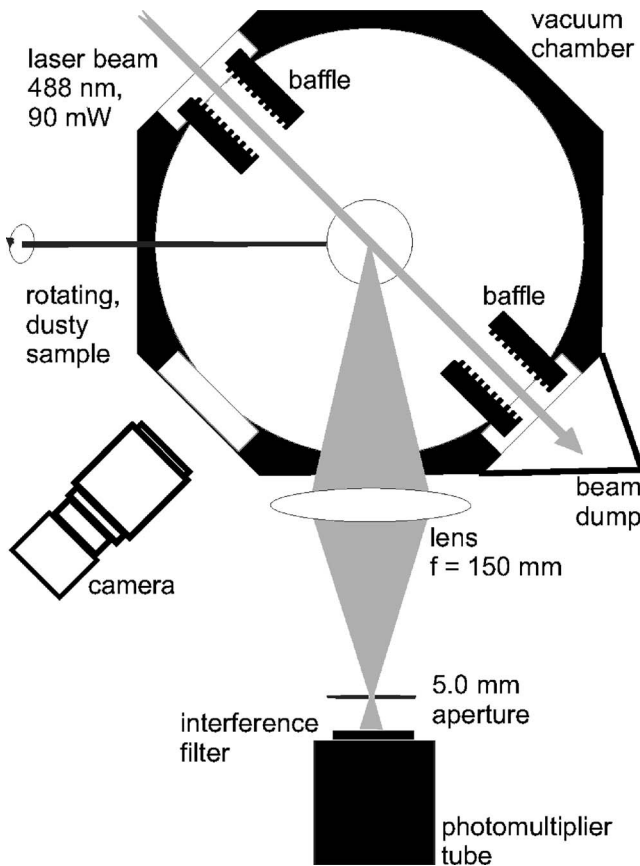


FIG. 4. Top view of laser-light scattering. Laser light scattered is detected at  $45^\circ$  by a photomultiplier tube, and at  $90^\circ$  by a video camera.

argon laser beam, with a Gaussian beam of 0.78 mm (measured as the full width at half-maximum), is positioned 10 mm above the sample, as shown in Fig. 3. This LLS configuration allows us to detect dust that is released in an upward direction, from the sample's upper hemisphere. This upper hemisphere is exposed to either the plasma, the electron beam, or both, depending on the experimental condition that is selected. Light scattered at  $45^\circ$  is detected by a photomultiplier tube (PMT), as shown in Fig. 4. The PMT is fitted with a 488 nm interference filter with a 3 nm bandwidth that blocks most of the white light from the tungsten filaments and neon spectral line emission. The PMT signal is digitized at 133 samples per second, providing a time series that is our primary measurement of the dust release rate. We also record two other time series: the discharge current time series (which indicates when the plasma was turned on), and the rotation sensor for the sample. As a visual indicator, we image the LLS at  $90^\circ$  using a video camera operated at 30 frames per second. Recording of these time series began shortly before turning the plasma on abruptly. The sample was not pretreated with any plasma or electron beam before beginning the data recording.

We select among our three experimental conditions, listed in Sec. III, by controlling the gas pressure and the position of a beam blocker. Experiments with only an electron beam are done at the base pressure of  $2 \times 10^{-6}$  Torr, while experiments with a plasma are performed at a neon gas pressure of 1 mTorr. When the plasma is on, we switch be-

tween experimental conditions with and without the electron beam by using the beam blocker, which is a  $10\text{ cm} \times 10\text{ cm}$  black-anodized plate. The blocker is inserted to obstruct the electron beam from direct exposure to the sample to achieve the condition with only a plasma. It is removed for the other two conditions. Only the upper hemisphere of the rotating sample faces the electron beam.

The gas pressure of 1 mTorr when operating with a plasma is so low that all collisional mean free paths are longer than both the sample and the sheath surrounding the sample. This condition allows us to use a collisionless sheath model as described in Sec. II. Collisional mean free paths range from 14 cm (for charge exchange) to 14 m (for ionization by impact of 70-eV electrons). These mean free paths are larger than the 4.5 cm sample diameter and the sheath thickness which ranges from 1 to 4 cm as calculated using the sheath model.

## V. RESULTS

We tested all three experimental conditions and found that only the condition of a plasma with an electron beam causes measurable dust release. This release nearly obeys an exponential time dependence, and the rate of release increases with plasma density. For the other two experimental conditions, we observed no measurable dust release. We next present these results in detail.

Tests for an electron beam only did not result in any measurable dust release. Neither the LLS signal nor the visual indication from video imaging indicated any release. If there were any release, it would be below our detection limit which is due to the small level of white light from the filaments that passed through our interference filter. We made an effort to make this detection limit as small as possible by using a black-anodized vacuum chamber and a narrow-bandwidth interference filter.

As explained above in Sec. IV, the sample is charged to  $V_{\text{float}}$  under these conditions with an electron beam only. In the absence of significant plasma density, the potential surrounding the sample is assumed to vary as  $1/r$ . For a  $V_{\text{float}} = -75$  V, we calculate the electric field at the sample's surface to be about 30 V/cm, directed inward. This combination of charging, electric field, and lack of any significant ambient thermal electron and ion density does not result in any measurable dust release.

Similarly, tests with a plasma only did not result in any measurable dust release. In this test, with the blocker inserted to obstruct the electron beam from impinging on the sample, we exposed the sample to plasma of density  $4 \times 10^6 \text{ cm}^{-3}$  for 4 min. During this exposure, neither the LLS signal nor the video indicate that there is any dust release.

The sample is charged under these conditions of plasma only, and it is also exposed to a sheath electric field at the sample's surface of 5 V/cm, directed inward, calculated using the collisionless sheath model. Under these conditions, the sample is exposed to significant ambient thermal electron and ion densities, but no electron beam. These conditions, including the charging and the sheath electric field, do not result in measurable dust release.

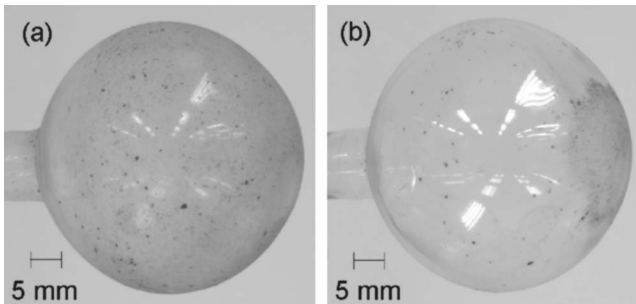


FIG. 5. (Color online) Photographs of the sample (a) before and (b) after plasma exposure. Before exposure, the sample was coated with  $\approx 80$  mg of JSC-1 simulant. Exposure to plasma lasted 4 min, with the electron beam unblocked. The plasma density was measured using a Langmuir probe in a plasma that was dust free, but otherwise had the same conditions as in this test, yielding  $n = 2.5 \times 10^8 \text{ cm}^{-3}$ . In a plasma with dust,  $n$  might be less, due to depletion, as discussed in the text.

Only tests with both a plasma and an electron beam resulted in dust release. These tests were done with the blocker withdrawn. Both the LLS signal and video imaging indicate significant dust release. A compelling demonstration of this release can be found by viewing the video.<sup>27</sup> From these tests, we can conclude that the required conditions for rapid release of particles are the presence of both a plasma and an electron beam. When the plasma is turned on, dust is released from the sample's surface and there is a large increase in the LLS signal. As the dust on the surface is depleted, the LLS signal diminishes in time.

Tests with a plasma and an electron beam were repeated with the plasma density  $n$  varied over two orders of magnitude, from  $2.4 \times 10^6$  to  $2.5 \times 10^8 \text{ cm}^{-3}$ . By varying  $n$ , we also varied both the sheath electric field and the rate at which thermal electrons and ions impinge on the sample. The maximum plasma density was limited by filament lifetime.

We found that significant dust release occurred at plasma densities above  $2.4 \times 10^6 \text{ cm}^{-3}$ . Below this density, we observed some release, but at a rate at least ten times smaller. Thus, we conclude that a threshold plasma density of about  $2.4 \times 10^6 \text{ cm}^{-3}$  must be exceeded for significant dust release under our experimental conditions.

As a cleaning method, we found that plasma exposure was best at high plasma densities. As a qualitative but compelling demonstration of cleaning, we photographed our sample before and after plasma exposure, using identical lighting conditions and camera exposure. The before and after photographs shown in Fig. 5 are for 4 min of plasma exposure at  $n = 2.5 \times 10^8 \text{ cm}^{-3}$  for a plasma with an electron beam. The sample was prepared with 80 mg of dust.

The importance of the electron beam is demonstrated by two results. First, we observed significant dust release for the experimental condition of plasma with an electron beam, and not for the condition with a plasma only. Second, in Fig. 5(b) we see that dust was not cleaned from a 2 cm diameter endcap on the right of the glass sphere. Unlike other portions of the sphere that sometimes directly faced the downward-pointing electron beam, this endcap always faced sideways so that it collected few beam electrons.

The electric field at the sample's surface ranged from 2

to 100 V/cm, calculated using Eq. (7), for tests with both a plasma and an electron beam. The highest electric field is achieved at the highest plasma density. This range of electric field overlaps the values of 5 and 30 V/cm that we estimated for the plasma-only and electron-beam-only conditions, respectively. Moreover, the range of plasma densities we tested with both plasma and electron beam include the value of  $4 \times 10^6 \text{ cm}^{-3}$  that resulted in no release for the condition with a plasma only.

From these results we can conclude that the values of the electric field and the plasma density by themselves cannot predict whether dust release will occur. A third requirement, in addition to a sufficient plasma density and electric field, is an electron beam. This finding completes our first goal of identifying the conditions required for dust release.

Our other two goals, verifying an inverse exponential time dependence and quantifying the dependence of the release rate on plasma density, require that we carefully prepare a time series for the LLS signal. The LLS time series for tests with four different plasma densities are shown in Fig. 6. Each row in this figure corresponds to a test with a different plasma density  $n$ . The left column shows the raw LLS signals. The right column shows the same data after applying a low-pass filter to smooth out rotational fluctuations and subtracting a baseline that is due to white light from the filaments. The baseline is calculated by averaging the raw LLS signal time series over the final 10 to 15 s, corresponding to a few sample rotations. For the low-pass filter, the data are continuously averaged over the sample's rotation period of 4.7 s. Our method of applying dust to the sample did not yield a perfectly uniform coating. Consequently, the sample's azimuthal variations in the dust coating cause fluctuations in the raw LLS signal, as the sample rotates. These fluctuations due to the sample's rotation are almost completely eliminated by the low-pass filter.

An exponential decay in the LLS signal is revealed as a straight line in the semi-logarithmic plots in Fig. 6. Release is initially nearly an exponential decay, as would be expected for Poisson statistics. This first stage of decay has a duration of two or more decades. Before the signal diminishes to the noise level, we can identify a second stage of decay that is slower. This second stage of decay is most easily detectable for higher plasma densities. A release time constant  $\tau$  for the release rate in the initial stage of exponential decay is obtained by fitting the entire LLS signal time series to an inverse exponential with a baseline,  $\text{LLS}(t) = b + \alpha \exp(-t/\tau)$ . In this fit, there are three free parameters: the release time constant  $\tau$ , the baseline  $b$ , and the amplitude  $\alpha$  of the time series. We fitted the raw and the smoothed forms of the LLS signal separately.

The release time constant  $\tau$  is our main result here, and its values are reported in each panel of Fig. 6. Our finding of a second stage of decay is an additional result; we have made no effort to identify the cause of this second stage or to determine whether it depends on the initial thickness of the dust coating.

The rate of dust release increases with the plasma density, as shown in Fig. 7. Data for the release time constant  $\tau$  versus  $n$ , plotted with log-log axes, fall mostly on a straight

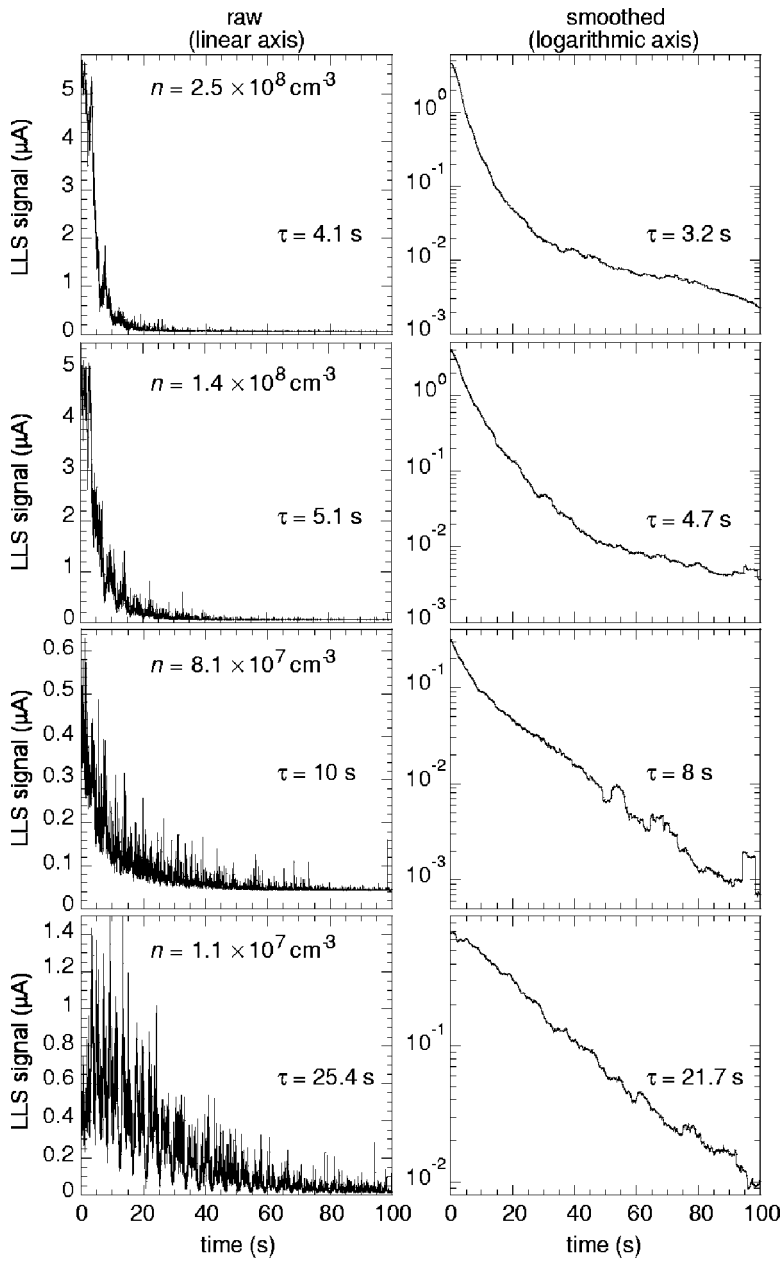


FIG. 6. Time series of the LLS signal for dust release from a glass sphere for four different plasma densities  $n$ . The left column is the raw LLS signal plotted on a linear axis, and the right column is the smoothed LLS signal plotted on a logarithmic axis. Each row of panels is for a different plasma density. The plasma is turned on at time  $t=0$ . The results of separately fitting the raw and smoothed LLS signals to an exponential decay are shown as the value of the release time constant  $\tau$ . In the right column only, a baseline due to white light is subtracted before plotting; these baselines are, from top to bottom, 0.0576, 0.0512, 0.0439, and 0.0135  $\mu\text{A}$ .

line, indicating a power-law scaling. Fitting the data in Fig. 7 to a power law  $\tau \propto n^{-p}$ , we find, as an empirical result, that  $p=0.628$ .

## VI. DUST RELEASE MECHANISM

We propose that dust release occurs, according to Poisson statistics, due to a fluctuating quantity. Because the time scale required for release is microseconds, estimated as the time required to move one contact distance due to a reasonable electric force, we can eliminate the subfemtosecond fluctuations associated with the van der Waals attraction as a candidate for the crucial fluctuation quantity. Instead, we consider the dust particle's charge, which can fluctuate significantly on the required millisecond time scale.

Thus, we propose that release occurs when a dust particle's charge fluctuates to a large negative value. At this large value, the electric force  $Q_{\text{dust}}E_{\text{sheath}}$  exceeds the adhesive

force. As we discussed in Sec. II, the charge of a dust particle adhered to a surface will fluctuate stochastically due to the collection of individual electrons and ions at random times. Moreover, we showed that the time-average charge on a single particle is far too small to overcome the adhesive force. Thus, it is essential to consider the fluctuations of the charge.

As was reported by Sheridan *et al.*,<sup>4</sup> an exponential decay of the dust release rate indicates that individual particles are released at random time intervals, with a constant probability per unit time. In this way, the release rate is simply proportional to the amount of dust remaining, and inversely proportional to a time constant that depends on the physical mechanism.

Here, we propose that the release mechanism requires a fluctuation of  $Q_{\text{dust}}$  beyond a threshold level corresponding to  $Q_{\text{dust}}E_{\text{sheath}} > F_{\text{vdW}}$ . This mechanism would result in dust re-

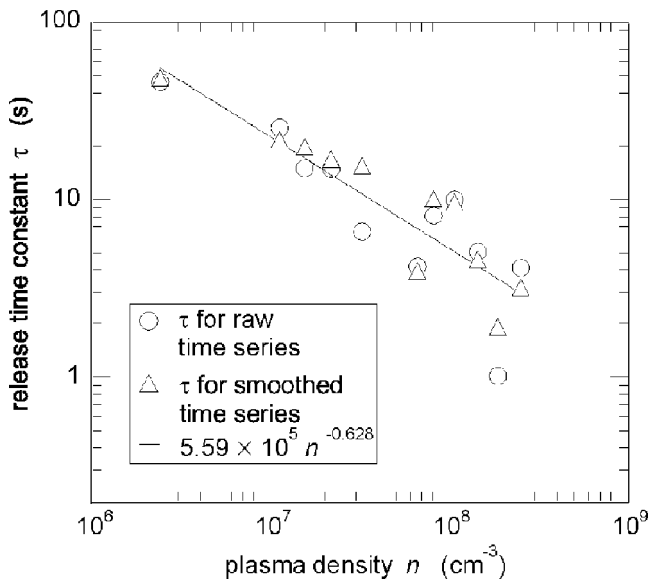


FIG. 7. Release time constant  $\tau$  vs plasma density  $n$ . Dust is released more rapidly at higher plasma densities. For each plasma density, we used a freshly prepared sample. The data fall on a straight line in this log-log plot, indicating a power law. The straight line shows the empirical fit result  $\tau_{\text{sec}}=5.59 \times 10^5 n^{-0.628}$ .

lease at a rate corresponding to the frequency at which  $Q_{\text{dust}}$  fluctuates beyond the threshold level. Since the fluctuations are due to the collection of individual electrons and ions, this frequency will be proportional to the plasma flux to the sample surface, and therefore the plasma density, if all other parameters are held constant. Thus, we would expect, as a signature of this mechanism, a release rate that increases with plasma density.

Our results that the release rate has a nearly exponential time dependence in the early stage, and that the release rate increases with the plasma density, are consistent with the stochastic mechanism described above. The nearly exponential time dependence is shown in Fig. 6, which also shows a slower second stage of particle release. We performed no tests to identify the reason for the second stage, although we speculate that it could arise from a combination of polydispersity of JSC-1 and a size dependence of the release rate. For the initial stage of release, our results from fitting the LLS signal to an exponential decay reveal that the release rate increases with plasma density, as shown in Fig. 7. This latter result is consistent with our proposed mechanism.

A slightly different mechanism that could also explain our results is a fluctuating dust-dust repulsion. Instead of requiring a sheath electric field to provide a force  $Q_{\text{dust}}E_{\text{sheath}}$  to overcome  $F_{\text{VDW}}$ , in this mechanism a binary Coulomb repulsion between two neighboring or touching dust particles would overcome  $F_{\text{VDW}}$ . This mechanism would again require that particle charges fluctuate, but the criterion would be that the product of two fluctuating charges should exceed a threshold. The fluctuations would arise for the same reason as in the model proposed above, due to the collection of individual electrons and ions from the plasma at random intervals. Therefore, this dust-dust mechanism would result in a release rate that increases with plasma density. Debye

shielding of the electric field between two neighboring dust particles could in some cases prevent this mechanism, but not in our case. This shielding would only happen if the Debye length  $\lambda_D$  is much smaller than the distance between neighboring dust particles.

The electron beam, which we found to be essential for dust release, most likely affects the charging mechanism. In our proposed mechanism where release occurs when  $Q_{\text{dust}}E_{\text{sheath}}$  fluctuates beyond a threshold, the electron beam can result in larger values of  $Q_{\text{dust}}$ . In the absence of a beam, a dust particle can fluctuate to a potential corresponding to only a small multiple of  $T_e/e$ . In our experiment,  $T_e$  is generally less than or near 10 eV, whereas the electron beam has an energy of 70 eV. This suggests that the threshold for release requires roughly tens of eV of potential on a dust particle.

## VII. PLASMA CLEANING

For the application of cleaning dusty surfaces by plasma exposure, our results indicate that a rapid rate of cleaning can be achieved. This is measured by the release time constant, which for our plasma source was as short as 1 s. Different plasma sources might allow higher plasma density and thereby provide an even faster cleaning rate.

The user might choose a different plasma. Our plasma source uses hot tungsten filaments, which has the disadvantages of high power consumption and deposition of evaporated tungsten. The user's plasma source should provide an electron beam along with the plasma. In addition, it should be operated at the highest practical plasma density, or at least above a threshold level that likely depends on the materials. There are many low-pressure plasma sources available, such as inductively coupled devices, that produce plasma densities that are as much as three orders of magnitude higher than ours, and we would expect that they would clean surfaces more rapidly, provided that they are accompanied by an electron beam.

## VIII. CONCLUSIONS

We have shown that dust particles adhered to surfaces can be released gradually when the surface is exposed to a plasma with an electron beam. For sufficient plasma densities, surfaces can be cleaned efficiently, which suggests applications in the semiconductor industry and spaceflight. The number of dust particles released from the surface varies exponentially in time when first exposed to a plasma with an electron beam. The time constant for this initial decay is shown to vary with plasma density according to a power law. We proposed a mechanism that requires that a particle charge  $Q_{\text{dust}}$  fluctuates stochastically until it exceeds a threshold, allowing the electric force to overcome the adhesive force. Our results suggest a need for a theoretical or simulation modeling of the time-dependent dust charging on the surface to better understand these random fluctuations.

## ACKNOWLEDGMENTS

The authors gratefully acknowledge helpful discussions of this paper with R. Merlino, V. Nosenko, T. Sheridan, and F. Skiff. We thank J. Colwell for providing JSC-1 lunar simulant.

This work was supported by NASA.

- <sup>1</sup>G. S. Selwyn, U. S. Patent No. 5,849,135 (15 December 1998).  
<sup>2</sup>G. S. Selwyn and I. Henins, U.S. Patent No. 6,546,938 (15 April 2003).  
<sup>3</sup>M. Horányi, Annu. Rev. Astron. Astrophys. **34**, 343 (1996).  
<sup>4</sup>T. E. Sheridan, J. Goree, Y. T. Chiu, R. L. Raider, and J. A. Kiessling, J. Geophys. Res. **97**, 2935 (1992).  
<sup>5</sup>B. Walch, M. Horányi, and S. Robertson, IEEE Trans. Plasma Sci. **22**, 97 (1994).  
<sup>6</sup>B. Walch, M. Horányi, and S. Robertson, Phys. Rev. Lett. **75**, 838 (1995).  
<sup>7</sup>M. Horányi, S. Robertson, and B. Walch, Geophys. Res. Lett. **22**, 2079 (1995).  
<sup>8</sup>M. Horányi, B. Walch, S. Robertson, and D. Alexander, J. Geophys. Res. **103**, 8575 (1998).  
<sup>9</sup>Z. Sternovsky, M. Horányi, and S. Robertson, J. Vac. Sci. Technol. A **19**, 2533 (2001).  
<sup>10</sup>Z. Sternovsky, S. Robertson, A. Sickafuse, J. Colwell, and M. Horányi, J. Geophys. Res. **107**, 5105 (2002).  
<sup>11</sup>J. N. Israelachvili, *Intermolecular and Surface Forces* (Academic, London, 1985), pp. 137–147.  
<sup>12</sup>V. A. Parsegian, *Van der Waals Forces* (Cambridge University Press, New York, 2006), pp. 24–27, 61.  
<sup>13</sup>G. Ziskind, M. Fichman, and C. Gutfinger, J. Aerosol Sci. **28**, 623 (1997).  
<sup>14</sup>M. Götzinger and W. Peukert, Langmuir **20**, 5298 (2004).  
<sup>15</sup>W. R. Bowen, N. Hilal, R. W. Lovitt, and C. J. Wright, Colloids Surf., A **157**, 117 (1999).  
<sup>16</sup>C. Arnas, M. Mikikian, and F. Doveil, Phys. Rev. E **60**, 7420 (1999).  
<sup>17</sup>S. Robertson, A. A. S. Gulbis, J. Colwell, and M. Horányi, Phys. Plasmas **10**, 3874 (2003).  
<sup>18</sup>C. Arnas, M. Mikikian, G. Bachet, and F. Doveil, Phys. Plasmas **7**, 4418 (2000).  
<sup>19</sup>C. Cui and J. Goree, IEEE Trans. Plasma Sci. **22**, 151 (1994).  
<sup>20</sup>T. E. Sheridan and J. A. Goree, IEEE Trans. Plasma Sci. **17**, 884 (1989).  
<sup>21</sup>D. S. McKay, J. L. Carter, W. W. Boles, C. C. Allen, and J. H. Allton, *Engineering, Construction, and Operations in Space IV* (American Society of Civil Engineers, Reston, VA, 1994), Vol. 2, 857–866.  
<sup>22</sup>B. M. Willman, W. W. Boles, D. S. McKay, and C. C. Allen, J. Aerosp. Eng. **8**, 77 (1995).  
<sup>23</sup>J. L. Klosky, S. Sture, H. Ko, and F. Barnes, J. Aerosp. Eng. **13**, 133 (2000).  
<sup>24</sup>J. Goree, Plasma Sources Sci. Technol. **3**, 400 (1994).  
<sup>25</sup>N. Hershkowitz, in *Plasma Diagnostics*, edited by O. Auciello and D. L. Flamm (Academic, San Diego, 1989), Vol. 1, Chap. 3, pp. 121–122.  
<sup>26</sup>V. A. Godyak, in *Plasma-Surface Interactions and Processing of Materials*, edited by O. Auciello, A. Gras-Marti, J. A. Valles-Abarca, and D. L. Flamm (Kluwer Academic, Dordrecht, 1990), pp. 95–102.  
<sup>27</sup>See EPAPS Document No. E-PHPAEN-13-029612 to view a video demonstrating dust release due to plasma exposure. This document can be reached via a direct link in the online article's HTML reference section or via the EPAPS homepage (<http://www.aip.org/pubservs/epaps.html>).